

LSST: Learned Single-Shot Trajectory and Reconstruction Network for MR Imaging

Hemant Kumar Aggarwal¹ Sudhanya Chatterjee¹ Dattesh Shanbhag¹
Uday Patil¹ K.V.S. Hari²

¹Advanced Technology Group, AI Organization, GE HealthCare, Bangalore India
{hemantkumar.aggarwal,sudhanya.chatterjee,dattesh.shanbhag,uday.patil}
@gehealthcare.com

²Center for Brain Research, Indian Institute of Science, Bangalore, India
hari@iisc.ac.in

Abstract

Single-shot magnetic resonance (MR) imaging acquires the entire k-space data in a single shot and it has various applications in whole-body imaging. However, the long acquisition time for the entire k-space in single-shot fast spin echo (SSFSE) MR imaging poses a challenge, as it introduces T2-blur in the acquired images. This study aims to enhance the reconstruction quality of SSFSE MR images by (a) optimizing the trajectory for measuring the k-space, (b) acquiring fewer samples to speed up the acquisition process, and (c) reducing the impact of T2-blur. The proposed method adheres to physics constraints due to maximum gradient strength and slew-rate available while optimizing the trajectory within an end-to-end learning framework. Experiments were conducted on publicly available fastMRI multichannel dataset with 8-fold and 16-fold acceleration factors. An experienced radiologist’s evaluation on a five-point Likert scale indicates improvements in the reconstruction quality as the ACL fibers are sharper than comparative methods.

1 Introduction

Magnetic Resonance (MR) Imaging is a non-invasive technique that offers superior soft-tissue contrast compared to other imaging modalities such as X-ray or CT. The quality of reconstructed images are influenced not only by the number of samples acquired but also by the sampling scheme employed. Therefore, optimizing the sampling pattern for acquisition is critical to further enhance the reconstruction quality [1, 2, 3, 4, 5, 6, 7, 8, 9].

Prior work exist regarding sampling pattern optimization scheme independent of reconstruction algorithm [1, 3, 4], active sensing techniques [10, 11] which optimizes sampling location after each TR, and methods that focus on multi-shot fast spin echo (FSE) sequences such as T2-Shuffling [12]. This study focuses on jointly optimizing sampling pattern and reconstruction network for single-shot spin echo MR imaging sequences.

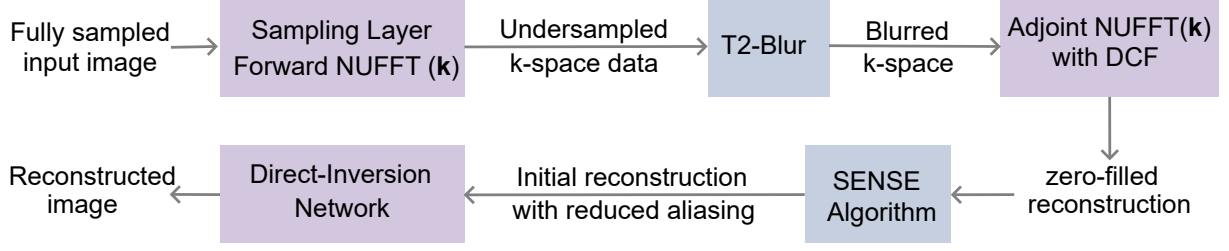
The process of undersampling k-space in two dimensions to expedite MR acquisition cannot be arbitrary due to practical considerations such as system configuration of gradient and slew-rate. Random undersampling, which necessitates swift gradient switching, is often impractical as it results in high eddy current-related artifacts [13]. When formulating a k-space trajectory, it’s crucial to consider the relevant MR system hardware constraints, specifically, the maximum gradient magnitude (G_{\max}) and maximum slew-rate (S_{\max}). These constraints limit the maximum velocity ($v_{\max} = \gamma G_{\max}$) and acceleration ($a_{\max} = \gamma S_{\max}$) of the trajectory, where γ is the Gyromagnetic ratio [14].

Given the benefits of arbitrary single-shot trajectories, this work focuses on optimizing them for a MR system with specific gradient and slew-rate specifications. This is achieved by determining the shortest path through a random initial set of points, akin to solving a Traveling Salesman Problem (TSP) [15]. A TSP trajectory might not meet the gradient constraints but provides a good initialization for the trajectory in the joint optimization framework.

Our approach improves upon the PILOT [16] study by eliminating the need for solving an explicit TSP during joint optimization. Unlike PILOT, this work explicitly accounts T2-Blur in single-shot acquisition and enhances reconstruction quality by incorporating the Density Compensation Factor (DCF) during training, and initializing the network input with a model-based solution. Unlike the BJORK [17] study, which doesn’t account for T2-blur, which is relevant for single-shot MR imaging, our method account for it. We propose a direct-inversion network to account for the unknown T2-Blur. Key contributions of this work include:

- Proposing an approach to accelerate 2D spin echo (SE) MR imaging as single-shot fast spin echo imaging, offering an effective alternative to the 1D undersampling approach that produces considerable aliasing and blurring artifacts for high acceleration rates.

(a) Training pipeline



(b) Inference pipeline

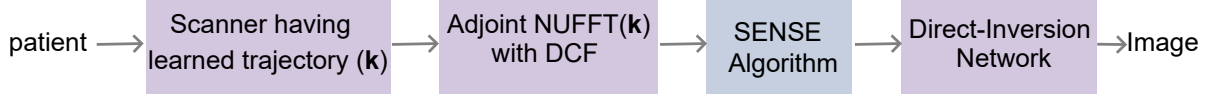


Figure 1: The training (a) and inference (b) pipeline of the proposed joint optimization framework. Here purple blocks contain trainable parameters.

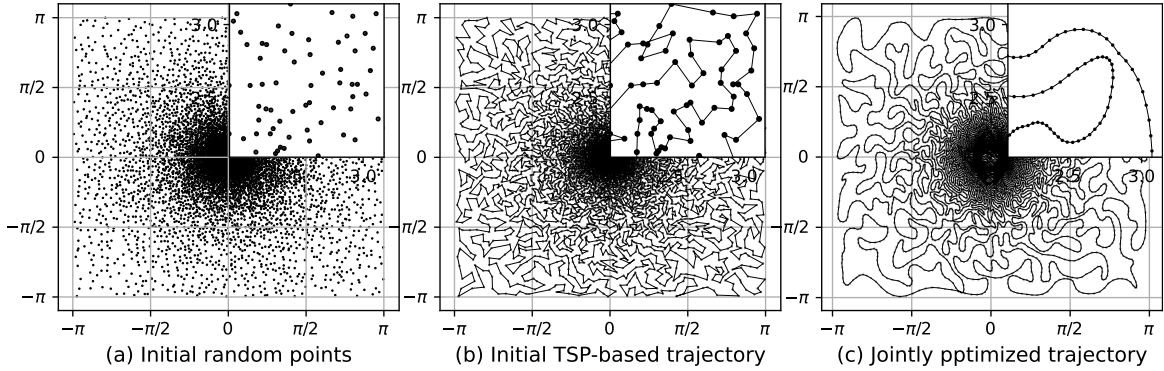


Figure 2: This figure (a) shows an example of a random set of points acquired to achieve an acceleration factor $R=8$. (b) shows corresponding TSP-based trajectory that does not satisfy physics constraints on maximum gradient strength and slew-rate. (c) shows optimized trajectory using the proposed LSST framework that has smooth curvature as seen from zoomed portions in range $[2\pi/3, \pi]$ that optimized trajectory has smooth curvature compared to (b) since it satisfy physics constraints.

- Development of a framework for accelerated single-shot MR image acquisition and reconstruction with a focus on reducing T2-Blur, noise, and aliasing artifacts occurring in single-shot fast spin echo imaging.
- Handling an unknown forward model in single-shot acquisition due to unknown T2-Blur, using a direct-inversion network. The T2 blur is simulated for the proposed imaging method in a physics aware manner.

2 Proposed Generalized Framework

Figure 1 illustrates the training and inference pipeline of our proposed Learned Single-Shot Trajectory (LSST) optimization framework, which concurrently optimizes both the k-space trajectory and the reconstruction network. Section 2.1 discusses trainable single-shot image acquisition model and section 2.2 discusses proposed joint optimization framework for trajectory optimization.

2.1 Trainable Single-shot Acquisition Model

Initially a random variable-density sampling mask for a given acceleration factor R is generated, as depicted in Fig. 2(a). An initial trajectory \mathbf{k} is generated from these random points using a TSP solver, such that the k-space center is sampled as the first point. The trajectory defines the order in which k-space is traversed to acquire the data in a single-shot. The network is initialized with this trajectory shown in Fig. 2(b). A direct TSP-based trajectory is infeasible since it does not satisfy physics constraints based on system hardware. Additionally, this generic trajectory is not necessarily optimal for a given dataset/task. Therefore, optimization of the trajectory is based on a given dataset while enforcing the physics constraints. Thus, trajectory is treated as a trainable parameter \mathbf{k} . After imposing these constraints, the learned trajectory has relatively smooth curvatures which are evident from Fig. 2(c).

As shown in Fig. 1(a), we input a fully sampled image \mathbf{x} to a backpropagation-compatible non-uniform Fourier transform (NUFFT) [17] operator $\mathcal{T}_{\mathbf{k}}$ to generate the undersampled k-space measurements \mathbf{y} using the forward model

$$\mathbf{y} = \mathcal{T}_{\mathbf{k}}(\mathbf{x}) + \mathbf{n}, \quad (1)$$

where \mathbf{n} is an additive Gaussian noise. Here, the operator $\mathcal{T}_{\mathbf{k}}$ consists of k-space sampling trajectory ($\mathbf{k} \in \mathbb{C}^m$), non-uniform Fourier transform, and coil sensitivity maps (CSM). This forward model is often considered in most image reconstruction and joint optimization frameworks including: [18, 2, 19, 17, 16, 18, 20]. However, this model (1) does not account for the T2-blur that is present in the single-shot MR acquisition. We can model this unknown tissue specific T2-blur in k-space as a following modulation operation

$$\mathbf{y}_b = \mathcal{B} \odot \mathbf{y}, \quad (2)$$

where \mathcal{B} represents the unknown k-space blur modulation function, and \mathbf{y}_b represent modulated, undersampled, and noisy measurements. Combining, (1) and (2), we get relatively accurate forward model for single-shot acquisition as

$$\mathbf{y}_b = \mathcal{B} \odot (\mathcal{T}_{\mathbf{k}}(\mathbf{x})) + \mathbf{n}. \quad (3)$$

The next section describes the reconstruction process from these acquired blurred noisy undersampled measurements \mathbf{y}_b .

2.2 Proposed Image Reconstruction Pipeline

This section describes the proposed three-step reconstruction process that involves initial iterative Sensitivity Encoding (SENSE) based reconstruction followed by deep learning based reconstruction and artifact reduction step.

2.2.1 Initial SENSE Reconstruction

Given that the trajectory densely samples the center of k-space and sparsely samples the periphery, it can introduce a bias towards the lower frequencies, resulting in a blurred reconstruction from the k-space measurements. Therefore, we explicitly account for density compensation prior to the reconstruction process. This work utilizes a backpropagation compatible implementation of a density compensation algorithm [21] on blurred measurements, \mathbf{y}_b , to obtain an approximation of regridding reconstruction, $\tilde{\mathbf{x}}$ using conjugate of the acquisition operator as $\tilde{\mathbf{x}} = \mathcal{T}_{\mathbf{k}}^*(\mathbf{y}_b)$.

The occurrence of blur in single-shot acquisition presents additional challenges due to the pronounced undersampling artifacts and get exacerbated at higher acceleration factors. Additionally, an unknown modulation function contributes to the blur in the reconstructed images (compounding the aliasing artifacts). The density compensated regridding reconstruction $\tilde{\mathbf{x}}$, obtained from blurred measurements \mathbf{y}_b , can be improved by using reconstruction algorithms such as Sensitivity Encoding (SENSE) that solves the following ℓ_2 -regularized optimization problem

$$\arg \min_{\mathbf{x}} \|\mathbf{y}_b - \mathcal{T}_{\mathbf{k}}(\mathbf{x})\|_2^2 + \lambda \|\mathbf{x}\|_2^2. \quad (4)$$

iteratively using Conjugate-Gradient algorithm, whose solution can be represented as

$$\mathbf{x}_0 = (\mathcal{T}_{\mathbf{k}}^* \mathcal{T}_{\mathbf{k}} + \lambda \mathcal{I})^{-1}(\tilde{\mathbf{x}}). \quad (5)$$

Although, due to the absence of blur information, single-shot forward model in (3) can not be directly used to obtain the solution \mathbf{x}_0 , still it acts as a good initial guess to the neural network since the aliasing artifacts are significantly reduced in \mathbf{x}_0 as compared to $\tilde{\mathbf{x}}$.

2.2.2 Direct-Inversion Network

Once we have an initial solution \mathbf{x}_0 , we can reconstruct the final image using a CNN. Unlike BJORK [17], the single-shot forward model (3) has unknown blur therefore a model-based deep learning approach is not directly applicable for the single-shot reconstruction and trajectory optimization. Therefore, in this work, we propose to reduce the artifacts present in \mathbf{x}_0 using a direct-inversion network such UNet [22]. It is possible to utilize a fixed feasible trajectory such as [23] and obtain the reconstructed image $\hat{\mathbf{x}}$ from \mathbf{x}_0 using deep learning methods as

$$\hat{\mathbf{x}} = \mathcal{D}_{\theta}(\mathbf{x}_0) \quad (6)$$

Here, \mathcal{D}_{θ} is a CNN with trainable parameters θ . This method only optimizes the network parameters once the samples are acquired. However, the joint optimization of the sampling trajectory (\mathbf{k}) and reconstruction network parameters (θ) can further improve the reconstruction quality. The joint optimization can be represented as

$$\hat{\mathbf{x}} = \mathcal{D}_{\theta, \mathbf{k}}(\tilde{\mathbf{x}}), \quad (7)$$

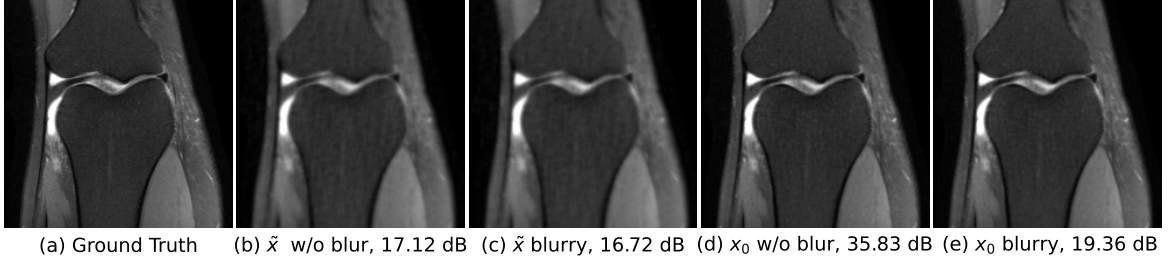


Figure 3: This figure contrasts analytic and iterative reconstructions used as network inputs. A fully sampled test image shown in (a) when undersampled at 8x and reconstructed using adjoint NUFFT with DCF results in (b). (c) and (d) depict iterative reconstructions via the SENSE algorithm, without and with blur in measurements, respectively. The blurred measurements lower the PSNR from 33.83 dB to 19.36 dB, highlighting the challenge of single-shot reconstruction.

where, $\mathcal{D}_{\theta, \mathbf{k}}$ represent the network that jointly optimizes trajectory and reconstruction parameters using the following loss function

$$\{\theta^*, \mathbf{k}^*\} = \arg \min_{\theta, \mathbf{k}} L_{\text{total}}(\hat{\mathbf{x}}, \mathbf{x}). \quad (8)$$

Here, \mathbf{x} represents the ground truth data and $L_{\text{total}} = L_{\text{task}} + \beta L_{\text{const}}$ is the total loss consisting of task loss L_{task} and constraint loss L_{const} with β as hyperparameter. L_{task} is a task-based loss function to minimize the error between ground truth and the reconstructed images. The L_{task} was considered as

$$L_{\text{task}} = \sum_{i=1}^N (||\hat{\mathbf{x}}_i - \mathbf{X}_i||_1 + (1 - \text{SSIM}(\hat{\mathbf{x}}_i, \mathbf{X}_i))), \quad (9)$$

where SSIM is the structural similarity index [24]. Here N represents the number of training images. However, solving (9) may make the trajectory infeasible while learning the trajectory for the MRI task. The gradient constraints are enforced by an additional constraint as proposed in [16]

$$L_{\text{const}} = \lambda_v \sum_{i=1}^{m-1} \max(0, |v_i| - v_{\text{max}}) + \lambda_a \sum_{i=1}^{m-2} \max(0, |a_i| - a_{\text{max}}), \quad (10)$$

with v_i and a_i as velocity and acceleration at i^{th} point, calculated using first and second derivatives of the trajectory as $\dot{\mathbf{k}}$ and $\ddot{\mathbf{k}}$, respectively.

The jointly trained network $\mathcal{D}_{\theta, \mathbf{k}}$ using the total loss function results in optimized trajectory \mathbf{k} and network parameters θ for a particular decimation rate (DR). We can acquire undersampled measurements using this optimized trajectory \mathbf{k} and later reconstruct the fully sampled image $\hat{\mathbf{x}}$ using this same network $\mathcal{D}_{\theta, \mathbf{k}}$ as shown in the inference pipeline in Fig. 1(b).

3 Experiments and Results

We trained and tested our models on a subset of parallel imaging fastMRI knee dataset [25] consisting of 100 volumes for training, 50 volumes for validation, and 94 volumes for testing. We performed network training on complex valued data at actual resolution without cropping. Images were cropped to center 320×320 only for display purpose. For simulating the single-shot data, we assumed, echo time (TE) = 100 ms, T2 for bone marrow fat = 80 ms, and sampling duration = 1 μ s. During loss function optimization, we set the value of gradient constraints as $G_{\text{max}} = 40\text{mT/m}$ and $S_{\text{max}} = 200\text{mT/m/ms}$.

3.1 Improved Input to the Network

Figure 3 highlights the impact of performing SENSE reconstruction using (5) with and without (w/o) considering the T2-Blur in the measurements. As we can see with a lower peak signal to noise ratio (PSNR) value of 19.36 dB in Fig. 3(d), the single-shot reconstruction problem becomes significantly challenging due to the presence of T2-blur. However, we note that the initial solution \mathbf{x}_0 (Fig. 3(d)) has reduced artifacts compared to $\tilde{\mathbf{x}}$ (Fig. 3(c)) and, therefore acts as a good initial input to the neural network.

3.2 Improved Reconstruction by the Network

We performed initial experiment using traditional compressed sensing algorithm [26] (1D undersampling) with a total variation regularization (CSTV) without accounting for the T2-Blur at 8x accelerated data acquired using uniform Cartesian sampling mask having 18 lines in the calibration region. In the second experiment, to

Table 1: Average PSNR (dB) and SSIM values at 8x and 16x acceleration factors shown as mean \pm standard deviation for 94 test subjects. Typically, higher average PSNR and SSIM values signify enhanced reconstruction quality. When compared to the classical CSTV reconstruction and the PILOT algorithm, our LSST approach yields superior PSNR and SSIM values for single-shot acquisition.

	PSNR		SSIM \times 100	
	8x	16x	8x	16x
CSTV	33.04 ± 1.06	30.91 ± 1.23	86.40 ± 2.32	82.46 ± 2.76
PILOT	36.49 ± 1.58	35.41 ± 1.44	91.88 ± 3.33	90.27 ± 3.78
Proposed	37.94 ± 1.89	36.17 ± 1.48	93.92 ± 2.69	91.82 ± 3.37

Table 2: Average Likert scores obtained for 20 volumes on five-point scale with scores as 1 to 5 include 1–non-diagnostic quality, 2–poor diagnostic quality, 3–fair diagnostic quality, 4–good diagnostic quality, 5–excellent diagnostic quality.

	SNR	Artifacts	Resolution	Contrast	Overall
Avg. of 20 volumes	5	5	4	5	5

ensure fair comparison, we extended the existing PILOT algorithm [16] to the single-shot settings accounting for T2-Blur in the measurements. In the third experiment, we implemented our proposed end-to-end training pipeline LSST as shown in Fig. 1(a).

Table 1 summarizes the PSNR and SSIM metrics on the test dataset at 8x and 16x acceleration factors for the three different methods previously discussed. Table 2 provides the quantitative evaluation results from an experienced radiologist on a five-point Likert scale. The evaluation metrics include SNR, Artifacts, Resolution, Contrast, and Overall Quality. It was observed that sharpness of ACL fibres was improved. The clinical implication for this is improved detection of partial ACL tears involving some of the fibres of the ACL. The proposed method scored highest primarily due to improvements in the ACL fibres being sharper while the meniscus region was found to be uniformly sharp across the different methods.

Figure 4 visually compares the reconstruction quality of CSTV, PILOT and LSST at 8x acceleration on a slice of a test subject. The zoomed regions indicate the improvement in the reconstruction quality. Appendix shows additional results on trajectory evaluation at 8x and 16x acceleration factors. Figure 7 in the appendix shows benefits of individual SENSE and DL components of proposed pipeline.

4 Conclusions and Discussions

This study introduces a method for the joint optimization of the k-space trajectory and reconstruction network parameters for single-shot acquisition that accounts for T2-Blur while adhering to MR system constraints. The learned trajectory meets gradient strength and slew-rate constraints and ensures practical trajectory estimation. Initial results and radiologist Likert scores affirm the method’s utility.

Acknowledgement

We thank Shriram KS for his help and support with the manuscript.

References

- [1] L. K. Senel, T. Kilic, A. Gungor, E. Kopanoglu, H. E. Guven, E. U. Saritas, A. Koc, and T. Çukur, “Statistically segregated k-space sampling for accelerating multiple-acquisition MRI,” *IEEE Transactions on Medical Imaging*, vol. 38, no. 7, pp. 1701–1714, 2019.
- [2] C. D. Bahadir, A. V. Dalca, and M. R. Sabuncu, “Learning-based optimization of the under-sampling pattern in MRI,” in *International Conference on Information Processing in Medical Imaging*. Springer, 2019, pp. 780–792.
- [3] J. P. Haldar and D. Kim, “OEDIPUS: An experiment design framework for sparsity-constrained MRI,” *IEEE Transactions on Medical Imaging*, 2019.
- [4] Y. Gao and S. J. Reeves, “Optimal k-space sampling in MRSI for images with a limited region of support,” *IEEE Transactions on Medical Imaging*, vol. 19, no. 12, pp. 1168–1178, 2000.

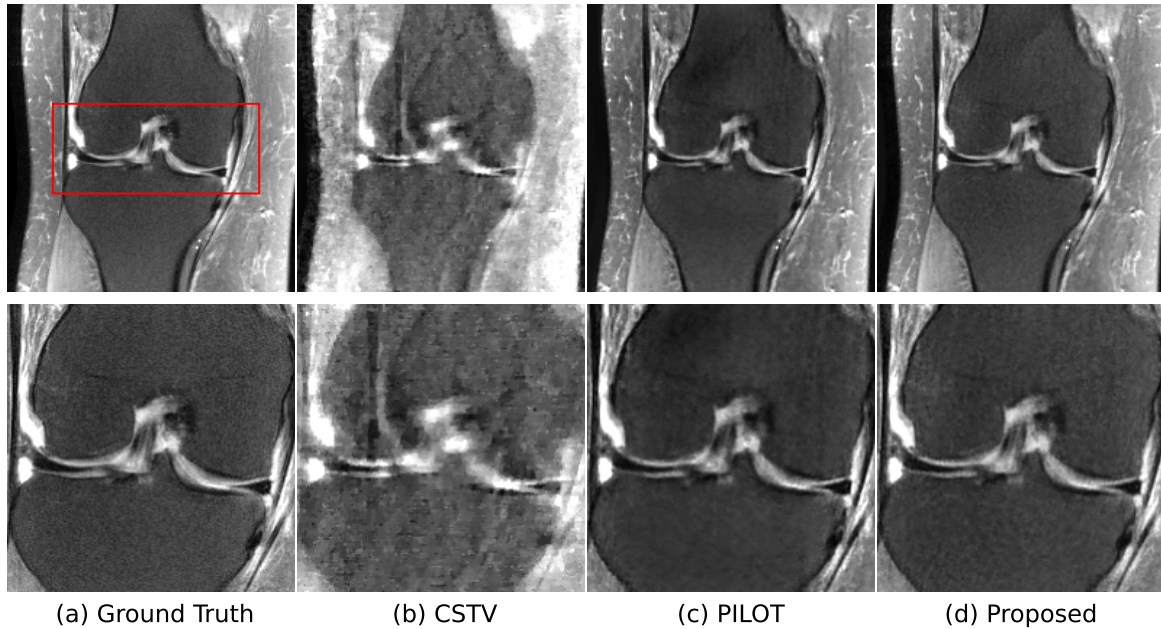


Figure 4: A comparison of experimental results at 8x acceleration on a test slice. The CSTV output (b) exhibits noticeable artifacts due to high 8x acceleration and the use of a 1D Cartesian sampling mask. The zoomed area shows that ACL fibers are sharper than PILOT (c) whereas meniscus is sharp everywhere in the proposed method (d).

- [5] F. Sherry, M. Benning, J. C. D. l. Reyes, M. J. Graves, G. Maierhofer, G. Williams, C.-B. Schönlieb, and M. J. Ehrhardt, “Learning the sampling pattern for MRI,” *arXiv preprint arXiv:1906.08754*, 2019.
- [6] B. Gözcü, R. K. Mahabadi, Y.-H. Li, E. Ilıcak, T. Çukur, J. Scarlett, and V. Cevher, “Learning-based compressive MRI,” *IEEE Transactions on Medical Imaging*, vol. 37, no. 6, pp. 1394–1406, 2018.
- [7] F. Liu, A. Samsonov, L. Chen, R. Kijowski, and L. Feng, “SANTIS: Sampling-augmented neural network with incoherent structure for MR image reconstruction,” *Magnetic resonance in medicine*, 2019.
- [8] T. H. Kim, B. Bilgic, D. Polak, K. Setsompop, and J. P. Haldar, “Wave-LORAKS: Combining wave encoding with structured low-rank matrix modeling for more highly accelerated 3D imaging,” *Magnetic Resonance in Medicine*, vol. 81, no. 3, pp. 1620–1633, 2019.
- [9] H. K. Aggarwal and M. Jacob, “J-MoDL: Joint model-based deep learning for optimized sampling and reconstruction,” *IEEE Journal of Selected Topics in Signal Processing*, vol. 14, no. 6, pp. 1151–1162, 2020.
- [10] K. H. Jin, M. Unser, and K. M. Yi, “Self-supervised deep active accelerated MRI,” *arXiv preprint arXiv:1901.04547*, 2019.
- [11] Z. Zhang, A. Romero, M. J. Muckley, P. Vincent, L. , and M. Drozdal, “Reducing uncertainty in under-sampled MRI reconstruction with active acquisition,” in *Proceedings of the IEEE Conference on Computer Vision and Pattern Recognition*, 2019, pp. 2049–2058.
- [12] J. I. Tamir, M. Uecker, W. Chen, P. Lai, M. T. Alley, S. S. Vasanawala, and M. Lustig, “T2 Shuffling: sharp, multicontrast, volumetric fast spin-echo imaging,” *Magnetic Resonance in Medicine*, vol. 77, no. 1, pp. 180–195, 2017.
- [13] S. Geethanath, R. Reddy, A. S. Konar, S. Imam, R. Sundaresan, R. B. DR, and R. Venkatesan, “Compressed sensing mri: a review,” *Critical Reviews™ in Biomedical Engineering*, vol. 41, no. 3, 2013.
- [14] R. B. Buxton, *Introduction to functional magnetic resonance imaging: principles and techniques*. Cambridge University Press, 2009.
- [15] N. Chauffert, P. Ciuciu, J. Kahn, and P. Weiss, “Travelling salesman-based variable density sampling,” *Proceedings of the 10th SampTA Conference*, pp. 509–512, 2013.
- [16] T. Weiss, O. Senouf, S. Vedula, O. Michailovich, M. Zibulevsky, and A. Bronstein, “Pilot: Physics-informed learned optimized trajectories for accelerated mri,” *Machine Learning for Biomedical Imaging*, vol. 1, pp. 1–23, 2021.

- [17] G. Wang, T. Luo, J.-F. Nielsen, D. C. Noll, and J. A. Fessler, “B-spline parameterized joint optimization of reconstruction and k-space trajectories (bjork) for accelerated 2d mri,” *IEEE Transactions on Medical Imaging*, vol. 41, no. 9, pp. 2318–2330, 2022.
- [18] K. Hammernik, T. Klatzer, E. Kobler, M. P. Recht, D. K. Sodickson, T. Pock, and F. Knoll, “Learning a variational network for reconstruction of accelerated MRI data,” *Magnetic Resonance in Medicine*, vol. 79, no. 6, pp. 3055–3071, 2018.
- [19] Yang, Yan and Sun, Jian and Li, Huibin and Xu, Zongben, “Deep ADMM-Net for compressive sensing MRI,” in *Advances in Neural Information Processing Systems 29*, 2016, pp. 10–18.
- [20] G. Yang, S. Yu, H. Dong, G. Slabaugh, P. L. Dragotti, X. Ye, F. Liu, S. Arridge, J. Keegan, Y. Guo *et al.*, “DAGAN: Deep de-aliasing generative adversarial networks for fast compressed sensing MRI reconstruction,” *IEEE Transactions on Medical Imaging*, vol. 37, no. 6, pp. 1310–1321, 2017.
- [21] J. G. Pipe and P. Menon, “Sampling density compensation in mri: rationale and an iterative numerical solution,” *Magnetic Resonance in Medicine: An Official Journal of the International Society for Magnetic Resonance in Medicine*, vol. 41, no. 1, pp. 179–186, 1999.
- [22] O. Ronneberger, P. Fischer, and T. Brox, “U-net: Convolutional networks for biomedical image segmentation,” in *International Conference on Medical image computing and computer-assisted intervention*. Springer, 2015, pp. 234–241.
- [23] S. Sharma, M. Coutino, S. P. Chepuri, G. Leus, and K. Hari, “Towards a general framework for fast and feasible k-space trajectories for MRI based on projection methods,” *Magnetic Resonance Imaging*, vol. 72, pp. 122–134, 2020.
- [24] Z. Wang, A. C. Bovik, H. R. Sheikh, and E. P. Simoncelli, “Image quality assessment: from error visibility to structural similarity,” *IEEE transactions on image processing*, vol. 13, no. 4, pp. 600–612, 2004.
- [25] J. Zbontar, F. Knoll, A. Sriram, M. J. Muckley, M. Bruno, A. Defazio, M. Parente, K. J. Geras, J. Katsnelson, H. Chandarana, Z. Zhang, M. Drozdal, A. Romero, M. Rabbat, P. Vincent, J. Pinkerton, D. Wang, N. Yakubova, E. Owens, C. L. Zitnick, M. P. Recht, D. K. Sodickson, and Y. W. Lui, “fastMRI: An open dataset and benchmarks for accelerated MRI,” in *ArXiv e-prints*, 2018.
- [26] M. Lustig, D. Donoho, and J. M. Pauly, “Sparse mri: The application of compressed sensing for rapid mr imaging,” *Magnetic Resonance in Medicine: An Official Journal of the International Society for Magnetic Resonance in Medicine*, vol. 58, no. 6, pp. 1182–1195, 2007.

5 Additional Results

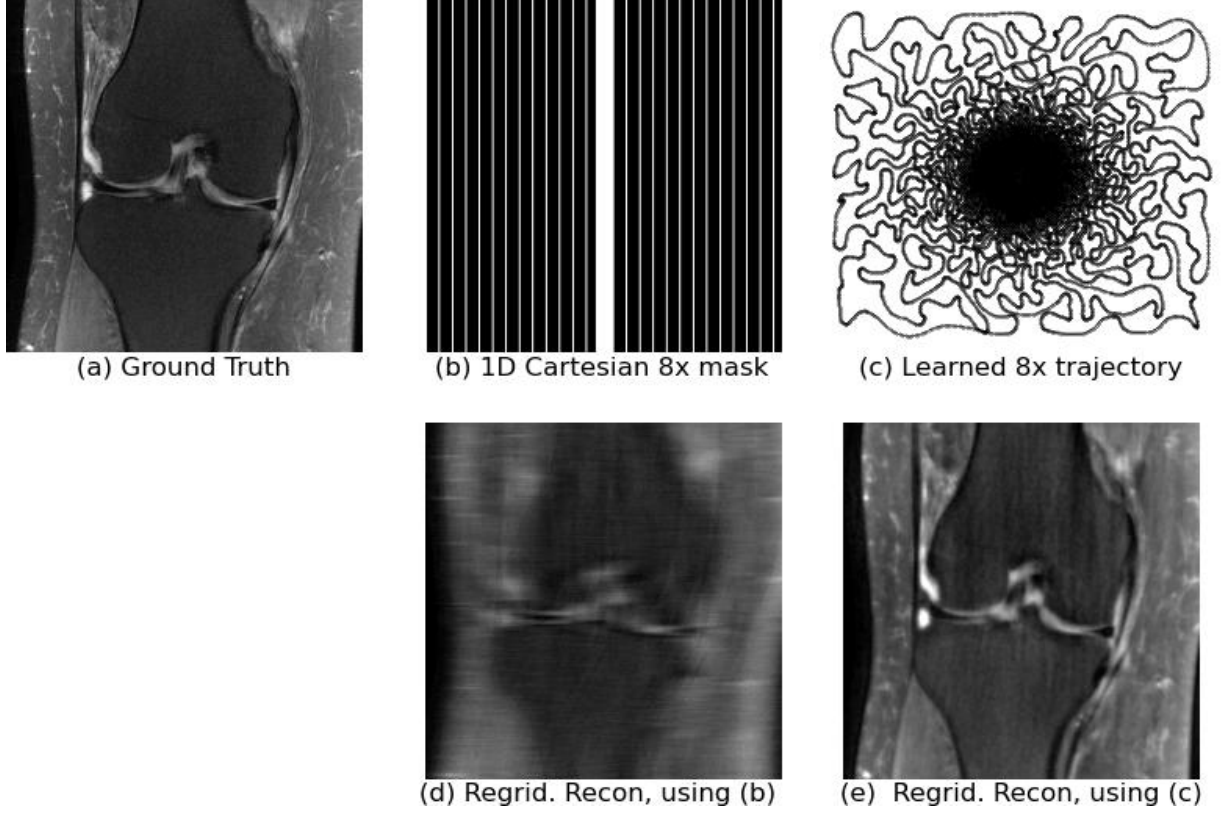


Figure 5: This figure shows the benefit of optimizing the trajectory rather than using traditional 1D Cartesian sampling to acquire the data. The ground truth image (a) was undersampled using mask in (b) and trajectory in (c) that resulted in undersampled k-space data which was reconstructed using regridding reconstruction (regrid. recon.) $\tilde{\mathbf{x}}$ to result in (d) and (e), respectively. Here, trajectory optimization also incorporated the T2-blur whereas Cartesian sampling experiment did not have additional blur. We note that (d) and (e) are not the final reconstruction but zero-filled reconstructions ($\tilde{\mathbf{x}}$) as shown in Fig 1(a). Since, (e) has many details as compared to (d), it can act as an improved input to the SENSE reconstruction block and subsequent neural network block.

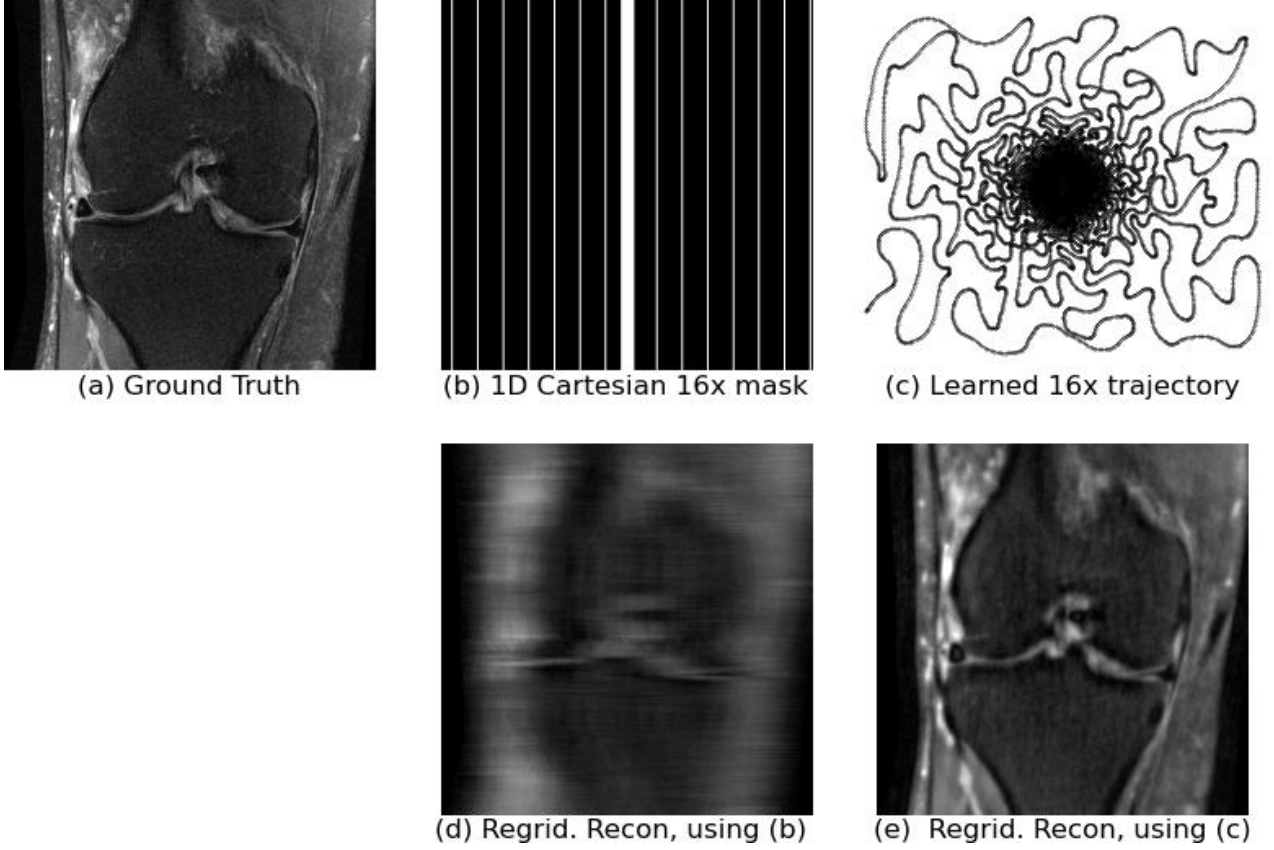


Figure 6: Same experiment as in Fig. 5 but at 16x acceleration factor. It can be noted from (e) that even at the 16x acceleration factor, some details are visible in the initial NUFFT based reconstruction. Here again we note that (d) and (e) are not final reconstructions but the regridding reconstructions $\tilde{\mathbf{x}}$ that goes as input to the SENSE block and subsequently to neural network block as shown in Fig 1(a).

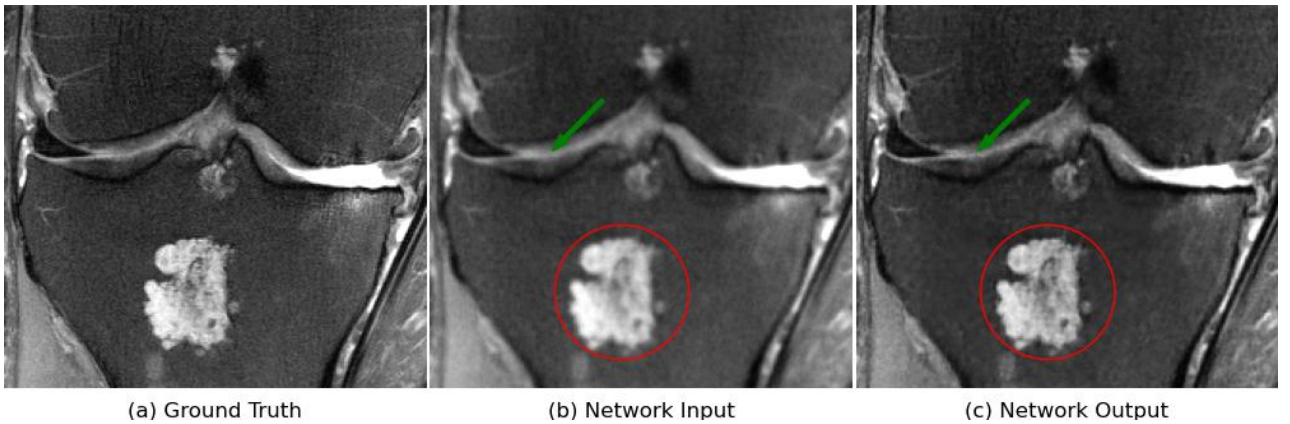


Figure 7: (a) is the ground truth fully sampled image. (b) is the output of SENSE algorithm on 8x undersampled and blurred measurements. The SENSE algorithm reduces the aliasing artifacts but does not reduce blur since the blur operator is unknown. This SENSE output acts as input to the direct-inversion network. (c) is the output of proposed network where blur is reduced significantly.

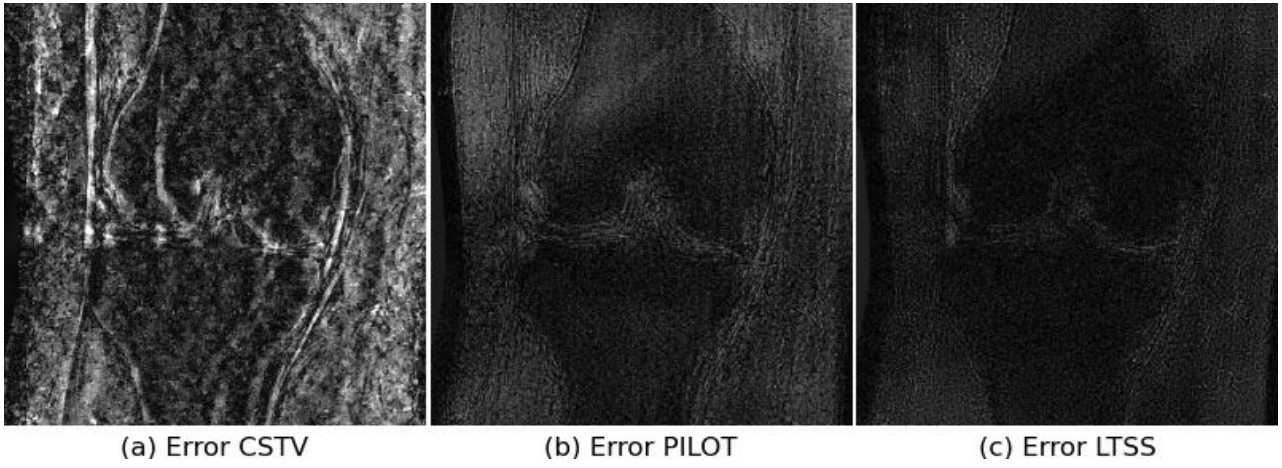


Figure 8: Error images between the ground truth image and reconstruction by different algorithms compared in Fig.4. The error maps are display range is adjusted for visualization purpose.